Confinement of $NaAlH_4$ in Nanoporous Carbon: Impact on H_2 Release, Reversibility, and Thermodynamics

Jinbao Gao,[†] Philipp Adelhelm,[†] Margriet H. W. Verkuijlen,[‡] Carine Rongeat,[§] Monika Herrich,[§] P. Jan M. van Bentum,[‡] Oliver Gutfleisch,[§] Arno P. M. Kentgens,[‡] Krijn P. de Jong,[†] and Petra E. de Jongh*[,†]

Inorganic Chemistry and Catalysis, Debye Institute for Nanomaterials Science, Utrecht University, Utrecht, The Netherlands, Institute for Molecules and Materials, Radboud University, Nijmegen, The Netherlands, and Leibniz Institute for Solid State and Materials Research (IFW Dresden), Dresden, Germany

Received: November 3, 2009; Revised Manuscript Received: January 25, 2010

Metal hydrides are likely candidates for the solid state storage of hydrogen. $NaAlH_4$ is the only complex metal hydride identified so far that combines favorable thermodynamics with a reasonable hydrogen storage capacity (5.5 wt %) when decomposing in two steps to NaH, Al, and H_2. The slow kinetics and poor reversibility of the hydrogen desorption can be combatted by the addition of a Ti-based catalyst. In an alternative approach we studied the influence of a reduced $NaAlH_4$ particle size and the presence of a carbon support. We focused on $NaAlH_4$/porous carbon nanocomposites prepared by melt infiltration. The $NaAlH_4$ was confined in the mainly 2−3 nm pores of the carbon, resulting in a lack of long-range order in the $NaAlH_4$ structure. The hydrogen release profile was modified by contact with the carbon; even for ∼10 nm $NaAlH_4$ on a nonporous carbon material the decomposition of $NaAlH_4$ to NaH, Al, and H_2 now led to hydrogen release in a single step. This was a kinetic effect, with the temperature at which the hydrogen was released depending on the $NaAlH_4$ feature size. However, confinement in a nanoporous carbon material was essential to not only achieve low H_2 release temperatures, but also rehydrogenation at mild conditions (e.g., 24 bar H_2 at 150 °C). Not only had the kinetics of hydrogen sorption improved, but the thermodynamics had also changed. When hydrogenating at conditions at which Na_3AlH_6 would be expected to be the stable phase (e.g., 40 bar H_2 at 160 °C), instead nanoconfined $NaAlH_4$ was formed, indicating a shift of the $NaAlH_4 \leftrightarrow Na_3AlH_6$ thermodynamic equilibrium in these nanocomposites compared to bulk materials.

1. Introduction

An important challenge for the use of hydrogen as an energy carrier is its compact and safe storage. A promising option is reversible storage in metal hydrides.[1] However, generally, metal hydrides exhibit too slow hydrogen release and uptake, and a too high thermodynamic stability.[2] Ideally, the enthalpy of the hydrogen release reaction should be in the range of 35−45 kJ/mol[H_2] to allow 1 bar of hydrogen release at proton exchange membrane (PEM) fuel cell operating temperatures. Sodium alanate ($NaAlH_4$) is the only complex metal hydride identified so far that combines a relatively high gravimetric hydrogen content with suitable thermodynamical properties. $NaAlH_4$ is known to decompose in three distinct steps (see Table 1).[2–5]

In practice, no hydrogen is released from undoped $NaAlH_4$ at 30−100 °C due to kinetic limitations. A small amount of hydrogen is released upon reaching the melting point (181 °C, the melting enthalpy is ∼25 kJ/mol), and most of the $NaAlH_4$ decomposes at higher temperatures. The decomposition of the hexahydride (Na_3AlH_6) typically starts at 240−250 °C. This leads to a second, clearly distinguishable, desorption step. The release of hydrogen in the third step is usually not considered, hence bulk $NaAlH_4$ maximally releases 5.5 wt % hydrogen. Once Al+NaH has been formed, absorption of hydrogen is very sluggish, requiring high pressures and extended periods of time. The kinetics for both H_2 desorption and absorption can be improved by the addition of a Ti-, Sc-, or Ce-based catalyst.[2–8] The mechanism is still a matter of intense debate, and only partial reversibility is achieved, which is ascribed to the irreversibility of the second decomposition step.

An alternative approach to enhance the kinetics is a decrease of the $NaAlH_4$ particle size even below 10 nm. Deposition of $NaAlH_4$ nanoparticles by solution impregnation of a support material led to X-ray amorphous materials[9,10] and an onset of hydrogen release even at room temperature, despite the absence of a metal-based catalyst. The improved kinetics were attributed to the effect of particle size.[11] Deposition using the same method in ordered mesoporous silica gave much higher hydrogen release temperatures.[10] In both cases, some reversibility was possible at milder conditions than for the bulk, but the reversibility was limited (rehydrogenation at 90 bar, 115 °C yielded 0.7 wt % H_2 on the second cycle;[9] 30 bar at 125 °C yielded 0.9 wt %[10]). Combined with the relatively low $NaAlH_4$ loadings that were achieved (1−10 wt % on carbon, maximum 20 wt % on SiO_2), this makes these systems less relevant for practical applications. More recently it was found that just the addition of small amounts of carbon (by ball-milling or simple physical mixing) also influenced the hydrogen release temperatures. However, the impact on hydrogen sorption properties was much less pronounced, and depended on the type of carbon material added.[12–14] Most recently, a paper has appeared on samples prepared by melt infiltration of porous carbon aerogels with

* To whom correspondence should be addressed. E-mail: P.E.deJongh@uu.nl.
[†] Utrecht University.
[‡] Radboud University.
[§] Leibniz Institute for Solid State and Materials Research.

10.1021/jp910511g
Published on Web 02/22/2010

TABLE 1: Steps in the Decomposition of $NaAlH_4$. Indicated Are the Amount of H_2 Released in This Individual Step, the Reaction Enthalpy, the Equilibrium Temperature under 1 Bar H_2 Pressure, and the Experimentally Observed Start of H_2 Release in Inert Atmosphere[2–5]

		wt% H_2	ΔH_r kJ/mol [H_2]	T_{eq} 1 bar H_2	$T_{release}$ in Ar
1	3 $NaAlH_4$ (s) ↔ Na_3AlH_6(s) + 2 Al(s) + 3 H_2(g)	3.7	37	30 °C	> 180 °C
2	Na_3AlH_6(s) ↔ 3 NaH(s) + Al(s) + 11/2 H_2(g)	1.85	47	100 °C	> 240 °C
3	NaH(s) ↔ Na(l) + 1/2 H_2(g)	1.85	56	425 °C	> 425 °C

$NaAlH_4$. The pore diameter was up to 20 nm, the $NaAlH_4$ showed XRD crystallinity. A strong enhancement of the kinetics of hydrogen release was observed, and reasonable reversibility was shown (reloading 4.6 wt % at 160 °C under 100 bar H_2 for 7 h).[15]

It is clear that carbon has a large impact on the hydrogen sorption properties of $NaAlH_4$. However, the nature of this interaction is not yet understood. Support effects are widely studied in heterogeneous catalysis, and physical effects of the support can roughly be distinguished in three groups:[16–18]

• *Electronic support effects*. These are most significant for small metal particles on ionic support materials, but are also postulated for small metal particles on carbon nanotubes.[19,20] Theoretical calculations indicate that the presence of π-electron density close to the graphene sheets might influence the ionic bonding strength between the Na^+ and AlH_4^- units in the $NaAlH_4$.[14] Electronic effects have a range limited to about 1−2 nm from the support.

• *Structural effects.* The support can induce and/or stabilize a certain size, shape and/or structure of the active phase. For instance, in the presence of a high surface area support, often nanoparticles are formed from a precursor, while without a support large crystallites of the active phase would be formed. This specific size, shape, or (lack of) crystallinity can have a strong influence on the functionality of the active phase. Kinetics can be enhanced by a large specific surface area, or shorter solid state diffusion distances. Furthermore, for small particles (<10 nm) the thermodynamics may be affected. To give an example, particle size effects are theoretically expected to have a strong influence on the enthalpy of formation of MgH_2 for particles smaller than 1−2 nm.[21,22]

• *Interface-related effects.* The fact that an interface between two phases is present can lead to several effects. If the bonding between support and active phase is strong and the support is mechanically robust, the active phase can be clamped (two-dimensional) or even confined (three-dimensional (3D), for instance, in pores of a support). Phase transitions such as (de)hydrogenation are commonly accompanied by a change in lattice structure and constants. Restraining the material can lead to internal stress, and hence to a change in thermodynamics.[23] Furthermore, kinetic effects can play a role, for instance nucleation of a phase transition might occur at the interface. These types of effects extend over distances typically much longer than 10 nm.

Apart from the physical support effects, specific chemical effects can also occur. For instance, the active hydrogen storage material might react with the support (e.g., $LiBH_4$ with SiO_2[24]), or intercalation of the metal phase can lead to a change in dehydrogenation enthalpy (e.g., NaH in porous carbon[25]).

In the present study, we discuss $NaAlH_4$/carbon composites, in which an intimate contact between the $NaAlH_4$ and the carbon is assured by melting the $NaAlH_4$ in the presence of the carbon. As a first system we study a well-defined graphite, for which a relatively thick layer of $NaAlH_4$ on the graphite surface is expected (∼10 nm assuming full wetting). Furthermore we study composites of $NaAlH_4$ with a porous carbon material, with mainly 2−3 nm pores. The main focus is on the nanocomposite system containing 20 wt % $NaAlH_4$, in which the $NaAlH_4$ is confined in the carbon nanopores, and as a result of this confinement lacks long-range structural order.[26] It is a challenge to characterize which phases are present: the active material is X-ray amorphous due to lack of long-range order, its high volability and reactivity make it rather unsuitable for high resolution electron microscopy, and the presence of a large amount of carbon seriously hampers spectroscopic methods. Hence, in addition to hydrogen sorption measurements, we employ high-pressure differential scanning calorimetry (HP-DSC) to monitor phase transitions, and ^{23}Na and ^{27}Al NMR to obtain a fingerprint of all the Na- and Al-containing components in the system, also upon de- and rehydrogenation steps. As the use of NMR is not straightforward, full details of the NMR characterization are published in a separate paper.[27]

2. Experimental Methods

High-purity porous carbon HSAG-500 (Brunauer−Emmett−Teller (BET) surface area 500 m^2/g and total pore volume 0.65 cm^3/g, broad pore size distribution with a maximum around 2−3 nm, 90 wt % of the particles <60 μm) was obtained from Timcal Ltd., Switzerland, as well as the nonporous graphite Timrex KS-6 (BET surface area 20 m^2/g, 0.07 cm^3/g pore volume). $NaAlH_4$ (>90%, Aldrich) was used as received, and no impurities were detected with ^{23}Na and ^{27}Al solid-state NMR. Before synthesis, the carbon support was dried at 500 °C for 4 h under an Ar flow. Typically, a total of 0.4 g of the carbon support material and 0.1g of $NaAlH_4$ were mixed in an Ar glovebox (Mbraun Labmaster I30, 2 ppm H_2O and <1 ppm O_2) and ground for 1 min in a mortar (20$NaAlH_4$/C). Melt infiltration was conducted in an autoclave (Parr 4836). The autoclave was loaded with ∼120 bar H_2 at room temperature, and heated first to 150 °C (3 °C min^{-1}, 15 min dwell time) and then to 180 °C (1 °C min^{-1}, 15 min dwell time), reaching 180−190 bar H_2 pressure at 180 °C. After cooling to room temperature, the pressure was released, and the autoclave was transferred to the glovebox, where the melt infiltrated sample was collected.

To release all hydrogen, melt infiltrated samples were placed in a flash-dried alumina cup (20 × 20 × 50 mm) and transported under an argon atmosphere to a tube furnace. The quartz tubes (ø50 × 1000 mm) in the furnace (Thermolyne 79300) had been predried at 200 °C under an Ar flow (30 mL/min). To limit evaporation, we placed the sample cup in a narrow alumina tube (ø 30 × 60 mm) inside the quartz tube. The sample was kept for 5 h with an Ar flow of 50 mL/min at 325 °C. After cooling to room temperature, samples were transferred to the glovebox under Ar atmosphere. Rehydrogenation was performed in the autoclave (Parr 4836) at 24 bar, 3 h, 150 °C; 40 bar, 15 h, 150 °C; 55 bar 15 h, 150 °C; and 180 bar, 12 h, 150 °C.

X-ray diffraction (XRD) patterns were obtained with a Bruker AXS D8 Advance 120 machine (Co K_α radiation) using an airtight sample holder. Nitrogen physisorption measurements were obtained at 77 K using a Micromeritics ASAP 2020. Barrett−Joyner−Halenda (BJH) pore size distributions were

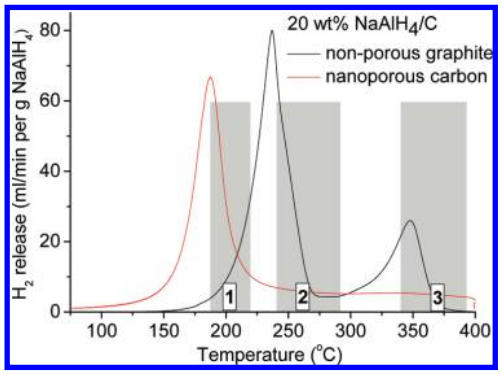

Figure 1. Hydrogen desorption from 20 wt % melt infiltrated $NaAlH_4$/C nanocomposites comparing a nonporous graphite and a nanoporous carbon material. The material was heated at 5 °C/min in Ar flow. Also indicated are the temperature regions for three different steps in the decomposition of bulk $NaAlH_4$ to (1) Na_3AlH_6, (2) NaH, and (3) Na and Al+H_2[26]

calculated using the adsorption branch of the isotherm. ^{23}Na and ^{27}Al magic angle spinning (MAS) NMR spectra were recorded using a Varian/Chemagnetics Infinity 600 MHz spectrometer with a 2.5 mm HX MAS probe. The single pulse excitation spectra were obtained using a short hard pulse of 0.20 μs at an effective radio frequency (RF)-field strength of 140 kHz after correcting for pulse rise and decay times, using sample spinning speeds of ~10 kHz.[27] HP-DSC measurements were obtained with an apparatus from Netzsch (DSC 204 HP Phoenix) at 120 bar H_2 operated in an Ar atmosphere glovebox, and heating and cooling at 5 °C/min.[28] Hydrogen release was studied by thermal programmed desorption under Ar flow (25 mL/min) using a Micromeritics AutoChem II equipped with a thermal conductivity detector (TCD). For measuring desorption and absorption cycles under hydrogen pressure, a magnetic suspension balance from Rubotherm was used. 100−200 mg of sample was put in an Inconel steel container, containing a 1−2 mm hole to allow equilibrium of the gas atmosphere, but not resulting in a direct gas flow through the sample bed. For hydrogen desorption the sample was heated to 300 °C at 1 °C/min under 1 bar H_2 flow (50 mL/min). For rehydrogenation, the temperature was lowered to 150 °C and the H_2 pressure was increased to 55 bar H_2 in about 3.5 h, with a dwell time of 30 min. After that, the sample was allowed to cool to 50 °C, and the pressure was decreased to 1 bar H_2, after which the next desorption run started.

3. Hydrogen Release from $NaAlH_4$/Carbon Nanocomposites

Figure 1 shows the hydrogen release for nanocomposites of 20 wt % $NaAlH_4$ with carbon prepared by melt infiltration, comparing a composite with nonporous graphite with one containing a nanoporous carbon material. Also indicated are the typical hydrogen release temperatures associated with the three steps in the decomposition of bulk $NaAlH_4$.[26]

For the composite with nonporous carbon, two major hydrogen release peaks are observed. The total amount of hydrogen released up to 400 °C is close to 7 wt % with respect to the $NaAlH_4$. This means that not only the first two decomposition steps, but also the third step (decomposition of NaH to Na and 1/2 H_2) was observed. The peak at 300−350 °C can clearly be attributed to the decomposition of NaH, as after heating to 300 °C crystalline NaH was observed, and a hydrogen release at 300−350 °C was also reported for NaH/porous carbon nanocomposites decomposed under the same conditions.[27] This implies that the decomposition of Na_3AlH_6 is not observed as a separate step in the desorption profile, in contrast with the situation for bulk and Ti-doped ball-milled $NaAlH_4$.

For the 20 wt % $NaAlH_4$ in the nanoporous carbon, an even larger impact on the hydrogen release temperatures was observed. The major peak has shifted to lower temperatures with hydrogen release starting already around 120 °C. Furthermore, no clear peak due to NaH decomposition is observed, although there is a continuous desorption of hydrogen at temperatures above 250 °C. Nanocomposites with porous carbon typically released 6.3 (±0.3) wt% H_2 with respect to the $NaAlH_4$ upon heating to 400 °C. This means that NaH must at least be partially decomposed at these temperatures. The fact that the first two decomposition steps combine into a single hydrogen release peak is intriguing, and has been reported before for crystalline $NaAlH_4$ contained in carbon aerogels.[15] It was then speculated that the kinetics for the second decomposition step of the Na_3AlH_6 to form NaH would be especially enhanced by the presence of the carbon. Also surprising is the disappearance of a well-defined decomposition step for the NaH. No crystalline NaH is observed in these samples after decomposition to 300 °C. Hence, a tentative explanation is that the second decomposition step results in such highly dispersed NaH that it decomposes over a wide temperature range, with decomposition starting at lower temperatures than crystalline NaH. Also, intercalation of Na upon decomposition could play a role in changing the thermodynamics for the decomposition of part of the NaH.[25]

Figure 2 shows the hydrogen release profiles for nanocomposites based on nanoporous carbon with $NaAlH_4$ loadings varying from 5 to 20 wt % (Figure 2a) and from 30 to 80 wt % (Figure 2b). For the lowest loadings (5−20 wt %), the profiles look very similar, with a well-defined, single release peak starting around 120 °C, and having a maximum hydrogen release rate around 180−190 °C under these conditions. The amount of hydrogen released per gram $NaAlH_4$ decreases for the lowest loadings, which is concomitant with the fact that a certain amount (rather than a certain fraction) of active material is lost during melt infiltration, handling, and storage.

For the 30 wt % loading, N_2 physisorption demonstrates that the vast majority of the $NaAlH_4$ is still present within the pores (see Figure S1 in the Supporting Information). For this sample, XRD detects a small amount of crystalline $NaAlH_4$, with an average crystallite size of 26 nm derived from the line broadening. It might well be that molten $NaAlH_4$ preferentially starts filling the smaller pores, and for the 30 wt % loading, some $NaAlH_4$ is also present in pores of 10−50 nm, which allow (partial) crystallization of the $NaAlH_4$. The major hydrogen release peak gradually shifts to higher temperatures with loading, a trend continued in the 40 and 50 wt % loading (not shown). For loading of 30 wt % and higher, coinciding with the onset of crystallinity, a separate peak due to NaH decomposition evolves. Above 40 wt % $NaAlH_4$ (at which point physisorption showed that the maximum amount that can be incorporated into the pores has been reached; see Figure S1), a well-defined peak due to NaH decomposition is observed, of which the position is further not significantly affected by the $NaAlH_4$ loading. Only for the very high loading of 80 wt % do additional shoulders in the hydrogen release profile become apparent, around 200 and 260 °C, which suggest that the sample partly shows bulk-like $NaAlH_4$ decomposition behavior. Remarkable is that a distinct hydrogen release profile is present for each individual sample. For instance for the 60 wt % sample, for which about 40 wt % of $NaAlH_4$ can be present inside the pores, and at least 20 wt

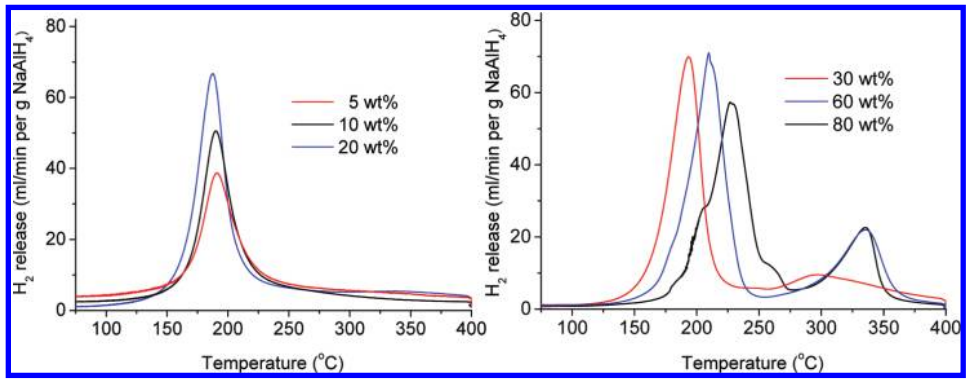

Figure 2. Hydrogen release from melt infiltrated $NaAlH_4$ nanocomposites with nanoporous carbon, and $NaAlH_4$ weight loadings ranging from 5 to 20 wt % (left) and from 30 to 80 wt % (right). Ar flow, heating with 5 °C/min.

% $NaAlH_4$ is present outside the pores, still a clear defined hydrogen release profile is observed, not a convolution of two profiles that can be ascribed to $NaAlH_4$ confined inside pores and $NaAlH_4$ on the outer surface of the carbon particle.

From the hydrogen release properties of these samples, we can deduce a few things about the origin of the differences with bulk $NaAlH_4$ decomposition. First, in the presence of nonporous graphite, as demonstrated in Figure 1, we can see that a single broad peak represents the first two decomposition steps of the $NaAlH_4$, with the average decomposition temperature being close to that of bulk $NaAlH_4$. A slight shift to lower temperatures of the NaH decomposition is observed. It is highly unlikely that direct electronic impact of the carbon plays an important role here, as the average layer thickness for this 20 wt % sample, assuming complete wetting of the carbon with the Alanate, is ~10 nm. Furthermore, the majority of the $NaAlH_4$ is crystalline (the crystallite size derived from line broading of the (112) diffraction line in XRD was 13 nm). It is also unlikely that a change in thermodynamics has occurred related to particle size effects or limited crystallinity of the active phase induced by the support. Hence, the change in hydrogen release properties for the composite with nonporous graphite is most likely due to kinetic effects, such as the $NaAlH_4$/carbon interface providing nucleation sites during phase transformation, or faster kinetics due to the larger specific surface area and shorter solid state diffusion distances in the active phase.

For the $NaAlH_4$ samples containing nanoporous carbon, quite different hydrogen desorption profiles are found (Figure 2), with a single clearly defined hydrogen release peak at lower temperatures. In this case, for samples up to 20−30 wt %, the $NaAlH_4$ is confined within the mainly 2−3 nm pores of the carbon, hence typically within 1−2 nm of the carbon surface. This means that, in addition to the kinetic effects mentioned above, thermodynamic changes might also have occurred due to loss of $NaAlH_4$ crystallinity, limited particle size, clamping, and/or electronic interaction with the carbon. This will be discussed in more detail in the following sections.

4. Reversibility of the Hydrogen Desorption

An important point with $NaAlH_4$ is the reversibility of the hydrogen sorption. For bulk samples it has been reported that virtually no hydrogen can be reabsorbed, even at 300 °C and 100 bar H_2, unless a metal-based catalyst is present.[2] However, recently for nanocomposites with carbon aerogels, reversibility was reported reloading at 160 °C under 100 bar H_2 for 7 h.[15] Figure 3 shows the hydrogen release for $NaAlH_4$/nanoporous carbon samples that were rehydrided at 150 °C at conditions of 24 bar up to 180 bar. For comparison, results for the composite

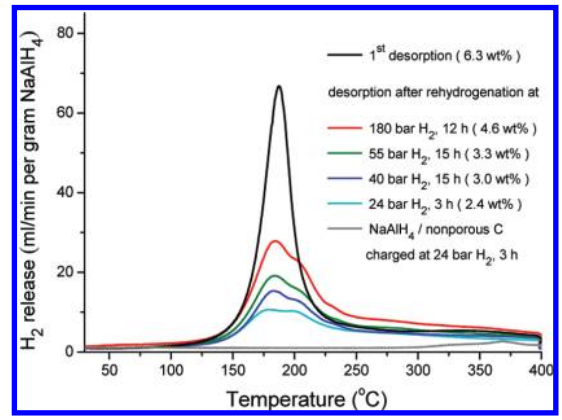

Figure 3. H_2 release for composites with nanoporous carbon containing 20 wt % $NaAlH_4$ after rehydrogenation under different conditions as indicated. H_2 desorption was measured under 25 mL/min Ar, heating with 5 °C/min to 400 °C followed by a 20 min dwell time. The quantity of $NaAlH_4$ released is indicated between brackets. For comparison, the 1st desorption is also shown, as well as results for the composite with nonporous graphite.

with nonporous graphite are also shown. In the latter case, virtually no hydrogen is released in the second dehydrogenation run, indicating that rehydrogenation under mild conditions is not possible. This means that the long-range interaction with the carbon that lowers the temperatures for hydrogen release from $NaAlH_4$ has no or a much more limited effect on the reverse reaction. In contrast, for the nanocomposites with the porous carbon, an appreciable amount of hydrogen is released after rehydrogenation at mild conditions. Although the profile has broadened, the peak position is roughly at the same temperatures as during the first desorption. The conditions used here are milder than those reported in literature so far for noncatalyzed alanates. For reloading at pressures up to 60−70 bar, from the bulk phase diagram (see Figure 7a) full reloading to $NaAlH_4$ is not expected, and the Na_3AlH_6 formed would theoretically release a maximum of 3.7 wt % H_2. After reloading at 55 bar, 3.3 wt % H_2 was released. This is a remarkably high number, especially considering the fact that the first desorption run had an efficiency of ~80%, and taking into account that the rehydrogenation procedure (transferring samples back to the glovebox after the desorption, and then to an autoclave, reloading them in the autoclave, and then via the glovebox again transfer them to the TPD equipment) inevitably comprises limited air exposure of the samples.

To avoid the oxidation associated with transfers, we studied the hydrogen cycling in a magnetically coupled microbalance. In this instrument we can measure under hydrogen pressure, as well as use slow heating rates, which allows us to approach

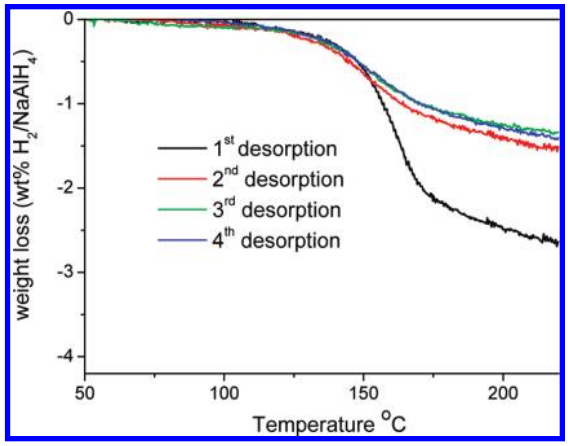

Figure 4. H_2 desorption from 20 wt % $NaAlH_4$ in nanoporous carbon for subsequent cycles under 1 bar H_2 flow and heating with 1 °C/min. Rehydrogenation was performed at 150 °C with a maximum pressure of 55 bar H_2.

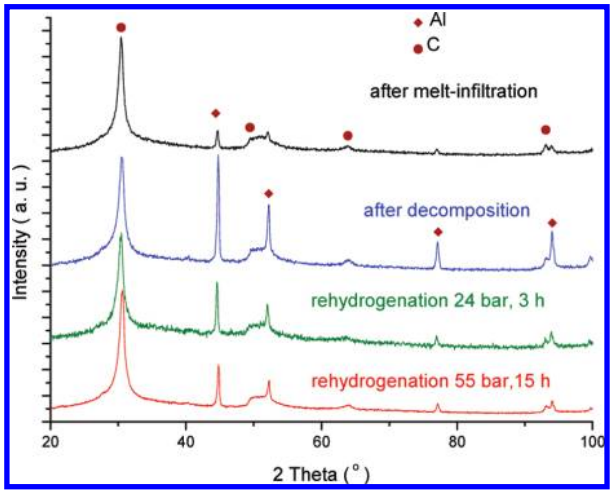

Figure 5. XRD patterns for the 20 wt % $NaAlH_4$/porous carbon nanocomposite, after melt infiltration, after decomposition at 325 °C for 5 h in Ar, and after rehydrogenation at 150 °C at different H_2 pressures and durations as indicated.

thermodynamic equilibrium. Figure 4 shows the hydrogen loss in subsequent cycles, while heating with 1 °C/min under 1 bar H_2 pressure. Hydrogen release starts around 100−120 °C, very comparable to the onset of hydrogen loss in Ar flow instead of 1 bar H_2. Most hydrogen is released below 170 °C, which is lower than in the TPD runs, probably due to the lower heating rate. The onset of hydrogen release under 1 bar H_2 is just above the temperature at which bulk Na_3AlH_6 at thermodynamic equilibrium decomposes under 1 bar H_2 (100 °C). NaH is not expected to decompose under 1 bar H_2 in this temperature range. Reloading was performed at 150 °C with a maximum pressure of 55 bar H_2. This yielded less hydrogen on the second desorption run than on the first which had been preceded by 180 bar H_2 pressure at 180 °C. However, upon further cycling, hardly any decay in capacity was observed, indicating very good partial reversibility and only limited loss of active material due to oxidation during measurement.

An intriguing aspect of this cycling under mild conditions is illustrated by the XRD patterns as shown in Figure 5. After melt infiltration, only peaks due to the carbon and a small amount of Al are observed. The crystalline Al is most likely formed by decomposition of a minor part of the macroscopic $NaAlH_4$ before it had a chance to melt infiltrate. Upon desorption of the hydrogen from the noncrystalline nanocomposite, more crystalline Al is observed. The crystallite size as derived from the peak width at half height using the Debye−Scherrer equation is 27 nm. This is in contrast with the microstructure of the $NaAlH_4$ that is included in the mainly 2−3 nm nanopores of the carbon and that does not show long-range order. The fact that larger Al crystallites are formed, which do not fit in the smallest pores of the carbon, indicates that the Al moves over relatively long distances. However, the major part of this process is reversible, as, upon rehydrogenation, the peak due to the crystalline Al decreases in height. Nevertheless, no crystalline $NaAlH_4$ is formed, indicating that upon hydrogenation the noncrystalline $NaAlH_4$ is reformed. It is difficult to image the large mobility of metallic Al at temperatures so far below its melting point of 660 °C. Several species have been theoretically proposed to contribute to the mobility of Al upon rehydrogenation and recombination with Na(H) to $NaAlH_4$, with one possibility being gaseous species such as AlH_3. However, given the results, it is safe to state that, although the migration of Al over large distances is probably the limiting factor in the reversibility of the hydrogen desorption from $NaAlH_4$, it seems that confining the $NaAlH_4$ in a nanoporous matrix at least limits the Al migration upon decomposition to such an extent that rehydrogenation is possible without a metal-based catalyst.

5. A Change in Thermodynamic Stability?

We have observed that, for the nanoconfined $NaAlH_4$, the hydrogen release starts well below the bulk melting point (181 °C[29]), while for undoped bulk $NaAlH_4$ only melting allows enough mobility within the undoped bulk phase to start the release of (a limited amount of) hydrogen. An important question is whether this is only related to a change in the kinetics of the hydrogen release reaction, or whether a change in thermodynamics might also be involved. It is known that the melting point of solid substances can be lowered by confining them into small pores, according to the Gibbs−Thomson equation. Hence a valid question is whether the melting point of $NaAlH_4$ in these composites might be lowered due to the nanoconfinement. A possible melting point depression was studied using DSC under high hydrogen pressure (120 bar H_2) and cycling between room temperature and 200 °C (see Figure 6).

The first heating cycle is not shown, as several heat effects take place simultaneously due to melting of the $NaAlH_4$, wetting of the carbon, infiltration of the pores, and possibly decomposition to Na_3AlH_4 or reaction with impurities of the carbon, all observed around the melting point. The second cycle is shown, upon heating to 200 °C (Figure 6a) a clear exothermic signal is observed for the composite with nonporous graphite. This can be ascribe to either the phase transformation of $NaAlH_4$ to Na_3AlH_6, or the melting of $NaAlH_4$, or most likely a combination of the two. Remarkably, for the nanoconfined $NaAlH_4$, no heat effect at all is observed. Also, upon subsequent cooling (Figure 6b), the composite with nonporous graphite shows a clear phase transition/solidification peak due to the presence of Na_3AlH_6/$NaAlH_4$, while no heat effects are distinguished at all for the nanocomposite between 200 °C and room temperature. It is documented that, for solids in pores, a large decrease in melting point can be observed, as well as a nonfrozen layer up to certain distances from the interface.[30] The extent of these effects is determined by the interfacial properties of the material involved. Hence the $NaAlH_4$ in nanoconfinement probably has a disordered structure. This is in agreement with the fact that no crystalline $NaAlH_4$ is observed with XRD, and implies that the enthalpy of formation of this nanoconfined noncrystalline phase is different from that of solid bulk $NaAlH_4$ (and shifted

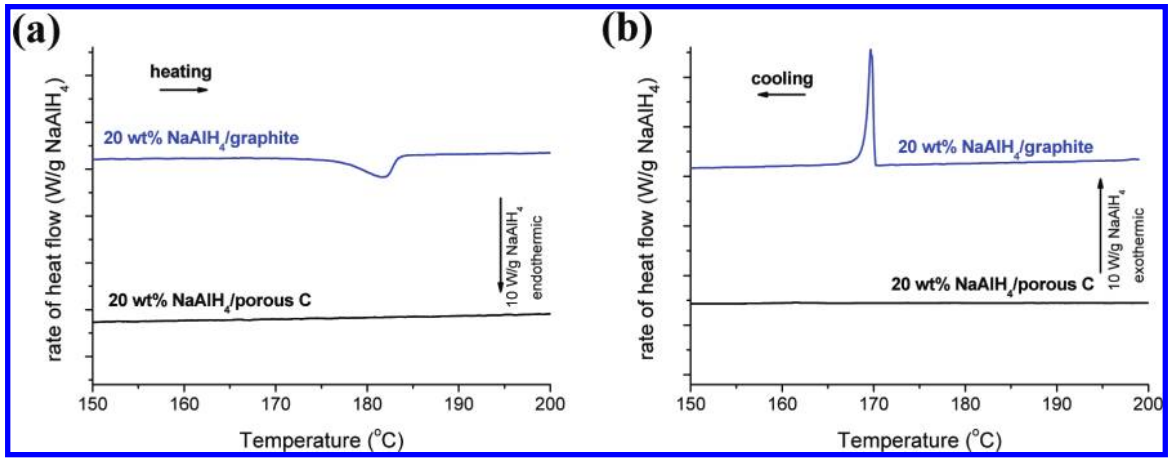

Figure 6. DSC comparing 20 wt % $NaAlH_4$ composites with porous carbon and nonporous graphite during (a) heating to 200 °C and (b) subsequent cooling with 5 °C/min under 120 bar H_2 pressure.

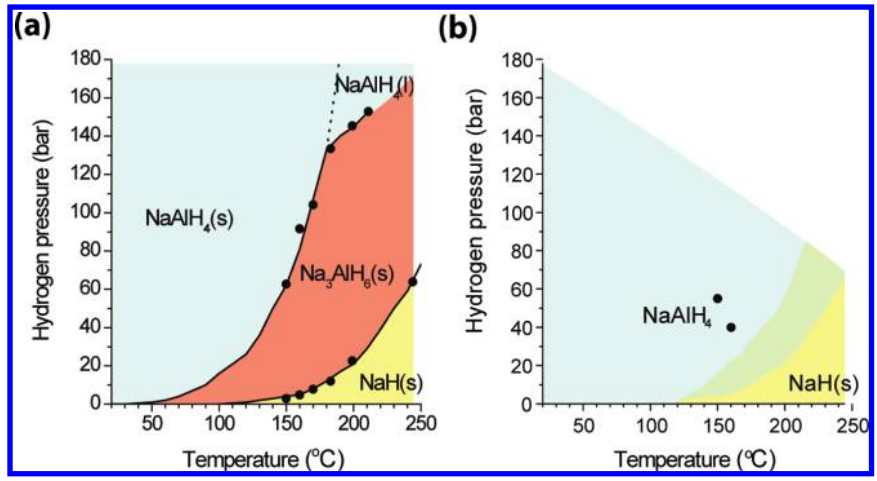

Figure 7. (a) Phase diagram for bulk $NaAlH_4$; dots indicate the measurement points (data from ref 31). (b) Indicative phase diagram for nanoconfined $NaAlH_4$. The rehydrogenation conditions are indicated with markers, at which the presence of $NaAlH_4$ and the absence of Na_3AlH_6 were measured with NMR.

toward that of liquid $NaAlH_4$). As the melting enthalpy of $NaAlH_4$ (~23−28 kJ/mol) is not much smaller than the decomposition enthalpy for $NaAlH_4$(s) to Na_3AlH_6(s) (37 kJ/mol) it means that possibly a significant change in dehydrogenation enthalpy might be expected. However, it can not *a priori* be derived what the impact on the thermodynamics of hydrogen release will be, as Na_3AlH_6 and NaH are also not detected as crystalline phases, hence the particle size and confinement effects do not only influence the thermodynamic stability of the $NaAlH_4$, but most likely also that of the decomposition products Na_3AlH_6, NaH, and Na. Another remarkable experimental observation is that no heat effect due to the phase transfer from $NaAlH_4$ to Na_3AlH_6 and the reverse is observed. According to the bulk phase diagram (Figure 7), this should occur around 170 °C. However, DSC shows no heat effects, and hence no phase transition when cooling from 200 °C to room temperature.

In none of the hydrogen desorption or rehydrogenation experiments was there any indication for the presence of Na_3AlH_6 as an intermediate phase in the decomposition, while for both bulk and Ti-catalyzed ball-milled $NaAlH_4$ this phase is readily observed upon partial decomposition or rehydrogenation. In the hydrogen release curves, the decomposition of $NaAlH_4$ into NaH or even Na seems to proceed in a single step, without any Na_3AlH_6 intermediate. NMR investigations of several partly desorbed nanocomposite samples never showed any presence of Na_3AlH_6, in contrast to measurements on the bulk $NaAlH_4$.[28] DSC heating and cooling of the composite sample with nonporous carbon under 120 bar H_2 showed a weak feature indicating the presence of some Na_3AlH_6 as evidenced by small heat effects due to the phase transformation around 245 °C (see Supporting Information, Figure S2), but not in the case of nanocomposites with porous carbon. As it seemed that Na_3AlH_6 could not be formed in any of the experiments, we wondered whether perhaps the stability region of Na_3AlH_6 in the phase diagram had changed. We are not aware of any experimental routes to prepare nanoconfined Na_3AlH_6. However, from theoretical calculations it is known that isolated AlH_6^- units show a degeneracy of electronic states around the Fermi level, leading to a large Jahn−Teller distortion and a relatively low stability. In bulk Na_3AlH_6, the local site symmetry is much lower than O_h, and hence the degeneracy is lifted, stabililizing the structure.[32] Figure 7a gives the bulk phase diagram for the Na, Al, H system, as derived from experimental measurements on Ti-doped and ball-milled $NaAlH_4$.[31]

We examined nanocomposites that previously had been dehydrogenated completely at 320 °C for 5 h. The conditions under which the dehydrogenated samples were rehydrogenated are indicated in Figure 7b (55 bar H_2 at 150 °C; 40 bar H_2 at 160 °C). Under these conditions partial rehydrogenation was achieved, as evidenced by the hydrogen release curves after rehydrogenation as shown in Figure 3. From the bulk phase diagram it is clear that, under the indicated conditions, Na_3AlH_6

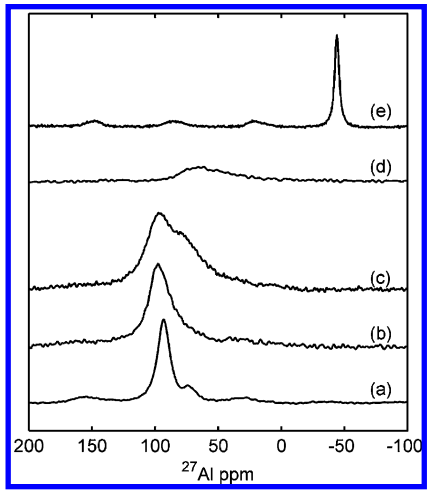

Figure 8. Solid-state ^{27}Al NMR spectra of samples containing 20 wt % $NaAlH_4$ and porous carbon: (a) physical mixture; (b) after melt infiltration; (c) after rehydrogenation at 160 °C for 15 h under 40 bar H_2; (d) dehydrogenated; and, as a reference, (e) a physical mixture of 20 wt % Na_3AlH_6/Al and porous carbon.

is the stable phase that should be formed, and formation of bulk $NaAlH_4$ from NaH (or Na), Al and H_2 is not possible under these conditions. As no crystalline phases other than Al were detected in our samples, we employed solid-state ^{27}Al NMR to evidence which phases were present. For the samples that had been rehydrogenated at 55 bar H_2, after rehydrogenation only nanoconfined $NaAlH_4$ and Al were identified, while no appreciable amount of Na_3AlH_6 was observed. For final proof we chose to rehydrogenate under 40 bar, 160 °C for 15 h, well into the region of the phase diagram where Na_3AlH_6 should be the stable phase. The relevant solid-state ^{27}Al NMR spectra are shown in Figure 8. For full details on the NMR characterization we refer to ref 27.

The physical mixture (curve a) shows the $NaAlH_4$ signal at 98 ppm (and two spinning side bands). The main feature is broadened, and the side bands have disappeared after melt infiltration (curve b). The small feature at 80 ppm is due to some aluminum oxides, which are formed during preparation and handling of the samples and which are insensitive to (de)hydrogenation. The intensity of this feature slightly increases upon further cycling and handling due to limited air exposure. After dehydrogenation, only metallic Al is formed (curve d, peak at 1635−1640 ppm outside the range of this figure). However, after rehydrogenation for 15 h at 160 °C and only 40 bar H_2 pressure, no Na_3AlH_6 was observed (curve c), as is clear from comparison with the Na_3AlH_6 reference spectrum (curve e). Apart from the Al, a clear signature due to the $NaAlH_4$ was found. Although this feature was slightly more broadened on the high field side (due to a limited amount of Al (hydr)oxides), it remarkably resembles the profile of the original nanoconfined $NaAlH_4$. In combination with the DSC results evidencing no phase transitions when cooling from 200 °C to room temperature under H_2 pressure, this unequivocally shows that the thermodynamic equilibria have shifted due to the nanoconfinement of the $NaAlH_4$, and that, in this case, a *stabilization* of the $NaAlH_4$ phase with respect to the Na_3AlH_6 phase was actually obtained, with decomposition occurring just above 100 °C under 1 bar H_2 (Figure 4). The single feature that is observed in the hydrogen release and the fact that no Na_3AlH_6 was detected in any of the experiments suggest that the Na_3AlH_6 region in the phase diagram has decreased significantly, or even disappeared.

6. Discussion and Conclusions

We conducted a study of the hydrogen sorption properties of nanocomposites of $NaAlH_4$ with nonporous and porous carbon. The presence of the carbon had a large impact on the hydrogen sorption properties, both on the release profile, the reversibility, and even the thermodynamics. The impact of the carbon can have different origins, and be related to electronic, structural, and/or interfacial effects. To trace the origin of the different effects, it is useful to systematically review the occurrence of these effects for three different types of melt infiltrated samples: the composite of 20 wt % $NaAlH_4$ with nonporous graphite (nominally forming a ∼10 nm thick $NaAlH_4$ layer on the carbon support), the nanocomposite with porous carbon (in which the $NaAlH_4$ is confined to mainly 2−3 nm pores, and as a result has no crystallinity), and the $NaAlH_4$/carbon aerogel system reported recently by Stephens et al.[15] in which the carbon is confined, but the pore size of 10−15 nm pores allows it to be crystalline.

The presence of carbon led to the following observations regarding the hydrogen sorption properties of $NaAlH_4$:

1. The hydrogen release profile was changed in the sense that the two first steps of the $NaAlH_4$ decomposition ($3NaAlH_4 \leftrightarrow Na_3AlH_6 + 2Al + 3H_2 \leftrightarrow 3NaH + 3Al + 6H_2$) were observed as a single step. This was the case for all three samples, regardless of whether the $NaAlH_4$ was confined in pores or on the outside of carbon particles, and regardless of whether the $NaAlH_4$ was crystalline or not. However, the dimensions of the $NaAlH_4$ phase did influence the exact peak position (the hydrogen release temperature), showing a gradual shift to lower temperatures with decreasing size. A similar shift to lower release temperatures with decreasing feature size was observed before for $NaAlH_4$ deposited from solution.[11] We can conclude that this shift is a kinetic effect, most likely related to shorter solid state diffusion distances and/or higher specific surface areas for the smaller particle/crystallite sizes.
2. The most strongly confined $NaAlH_4$ (in 2−3 nm rather than 10−15 nm diameter pores) showed the lowest hydrogen release temperatures (with hydrogen release starting at 100−120 °C, even under 1 bar H_2). Only for these samples was no distinct feature due to the decomposition of NaH observed in the hydrogen release profile. This can be related to structural effects: while for the other samples crystalline $NaAlH_4$ was decomposed via crystalline Na_3AlH_6 and crystalline NaH, for these samples no crystalline phases except Al were detected during the decomposition process. A very high dispersion of the NaH would explain the decomposition of this compound to start at low temperatures and the absence of a well-defined hydrogen release peak.
3. The hydrogen absorption was strongly enhanced for the samples in which the $NaAlH_4$ was confined in nanopores, but not for the composite with nonporous graphite. We observed that even for the $NaAlH_4$ confined in 2−3 nm pores, the Al formed upon decomposition had a strong tendency to sinter, leading to 25−30 nm large crystallites. Surprisingly upon rehydro under mild conditions, the XRD signature of these large Al crystallites disappeared and amorphous $NaAlH_4$ was reformed. This implies that the Al is mobile over relatively long distances. However, it can be concluded that the confinement of the phases in 3D nanopores (whether mainly 2−3 or 10−15 nm sized) is essential to restrict this mobility to such an extent that

rehydrogenation of a major part of the material at mild conditions is possible.

4. For the first time, we observed a strong change in thermodynamic properties: the $NaAlH_4$ showed an increased stability region, at the expense of the Na_3AlH_6 stability region in the phase diagram. NMR identified the presence of nanoconfined $NaAlH_4$ rather than Na_3AlH_6 under rehydrogenation conditions at which, according to the phase diagram, Na_3AlH_6 should be formed (for instance 160 °C and 40 bar H_2), indicating that the Na_3AlH_6 stability region has either decreased significantly or even disappeared. This effect is only found for $NaAlH_4$ confined in the smallest pores. For these samples, DSC measurements under 120 bar H_2 pressure showed no indication of heat effects in the temperature range up to 250 °C. This means that not only the $NaAlH_4 \leftrightarrow Na_3AlH_6$ phase transition is not observed, but also no melting and crystallization of the $NaAlH_4$ phase is seen. It can at present not be excluded that electronic interaction with the carbon plays a role (as the $NaAlH_4$ is within 1−2 nm of the interface), which could be verified by confining the $NaAlH_4$ in a material with similar pore size, but different electronic properties than carbon. However, given the result, it is most likely that the shift of the $NaAlH_4 \leftrightarrow Na_3AlH_6$ phase boundary is related to the intrinsic impact of the nanofinement on the thermodynamic potentials of the $NaAlH_4$ and Na_3AlH_6 phases.

Acknowledgment. We thank Timcal Ltd., Bodio, Switzerland, for providing the porous carbon material, and Rien van Zwienen for the gravimetric measurements. We acknowledge NWO-ACTS and a NWO-Vidi grant (016.072.316) for financial support, as well as the EU-RTN project (COSY) and HGF project (FuncHy).

Supporting Information Available: Overview of the N_2 physisorption results for $NaAlH_4$/nanoporous carbon composites with different $NaAlH_4$ loadings (Figure S1) as well as a DSC traces suggesting the presence of Na_3AlH_6 in the composite with nonporous graphite (Figure S2). This material is available free of charge via the Internet at http://pubs.acs.org.

References and Notes

(1) Schlapbach, L.; Züttel, A. *Nature* **2001**, *414*, 353.
(2) Bogdanovič, B.; Schwickardi, M. *J. Alloys Compd.* **1997**, *1*, 253–254.
(3) Gross, K. J.; Thomas, G. J.; Jensen, C. M. *J. Alloys Compd.* **2002**, *683*, 330–332.
(4) Felderhoff, M.; Weidenthaler, C.; von Helmolt, R.; Eberle, U. *Phys. Chem. Chem. Phys.* **2007**, *9*, 2643.
(5) Sakintuna, B.; Lamari-Darkrim, F.; Hirscher, M. *Int. J. Hydrogen Energy* **2007**, *32*, 1121.
(6) Orimo, S.-I.; Nakamori, Y.; Eliseo, J. R.; Züttel, A.; Jensen, C. M. *Chem. Rev.* **2007**, *107*, 4111.
(7) Wang, J.; Ebner, A. D.; Prozorov, T.; Zidan, R.; Ritter, J. A. *J. Alloys Compd.* **2005**, *395*, 252.
(8) Rongeat, C.; Llamas-Jansa, I.; Oswald, S.; Schultz, L.; Gutfleisch, O. *Acta Mater.* **2009**, *57*, 5563.
(9) Baldé, C. P.; Hereijgers, B. P. C.; Bitter, J. H.; de Jong, K. P. *Angew. Chem., Int. Ed.* **2006**, *45*, 3501.
(10) Zheng, S.; Fang, F.; Zhou, G.; Chen, G.; Ouyang, M.; Zhu, M.; Sun, D. *Chem. Mater.* **2008**, *20*, 3954.
(11) Baldé, C. P.; Hereijgers, B. P. C.; Bitter, J. H.; de Jong, K. P. *J. Am. Chem. Soc.* **2008**, *130*, 6761.
(12) Pukazhselvan, D.; Gupta, B. K.; Srivastava, A.; Srivastava, O. N. *J. Alloys Compd.* **2005**, *403*, 312.
(13) Cento, C.; Gislon, P.; Bilgili, M.; Masci, A.; Zheng, Q.; Prosini, P. P. *J. Alloys Compd.* **2007**, *437*, 360.
(14) Berseth, P. A.; Harter, A. G.; Zidan, R.; Blomqvist, A.; Moyses Araujo, C.; Scheicher, R. H.; Ahuja, R.; Jena, P. *Nano Lett.* **2009**, *9*, 1501.
(15) Stephens, R. D.; Gross, A. F.; Van Atta, S. L.; Vajo, J. J.; Pinkerton, F. E. *Nanotechnology* **2009**, *20*, 204018.
(16) Goodman, D. W. *Chem. Rev.* **1995**, *95*, 523.
(17) Gates, B. C. *Chem. Rev.* **1995**, *27*, 511.
(18) Campbell, C. T. *Surf. Sci. Rep.* **1997**, *27*, 1.
(19) Mojet, B. L.; Miller, J. T.; Ramaker, D. E.; Koningsberger, D. C. *J. Catal.* **1999**, *186*, 373.
(20) Pan, X.; Fan, Z.; Chen, W.; Ding, Y.; Luo, H.; Bao, X. *Nat. Mater.* **2007**, *6*, 507.
(21) Wagemans, R. W. P.; van Lenthe, J. H.; de Jongh, P. E.; van Dillen, A. J.; de Jong, K. P. *J. Am. Chem. Soc.* **2005**, *127*, 16675.
(22) Cheung, S.; Deng, W.-Q.; van Duin, A. C. T.; Goddard, W. A., III. *J. Phys. Chem. A* **2005**, *109*, 851.
(23) Baldi, A.; Gonzalez-Silveira, M.; Palmisano, V.; Dam, B.; Griessen, R. *Phys. Rev. Lett.* **2009**, *102*, 226102.
(24) Mosegaard, L.; Møller, B.; Jørgensen, J.; Filinchuk, Y.; Cerenius, Y.; Hanson, J. C.; Dimasi, E.; Besenbacher, F.; Jensen, T. R. *J. Phys. Chem. C* **2008**, *112*, 1299.
(25) Adelhelm, P.; de Jong, K. P.; de Jongh, P. E. *Chem. Commun.* **2009**, 6261.
(26) Adelhelm, P.; Gao, J.; Verkuijlen, M. H. W.; Rongeat, C.; Herrich, M.; van Bentum, P. J. M.; Gutfleisch, O.; Kentgens, A. P. M.; de Jong, K. P.; de Jongh, P. E. accepted for publication in *Chem. Mater.* (2010).
(27) Verkuijlen, M. H.W.; Gao, J.; Adelhelm, P.; van Bentum, P. J. M.; de Jongh, P. E.; Kentgens, A. P. M. *J. Phys. Chem. C* DOI: 10.1021/jp911228x.
(28) Rongeat, C.; Llamas-Janse, I.; Doppiu, S.; Delledda, S.; Borgschulte, A.; Schultz, L.; Gutfleisch, O. *J. Phys. Chem. B* **2007**, *111*, 13301.
(29) Claudy, P.; Bonnetot, B.; Chahine, G.; Letoffe, J. M. *Thermochim. Acta* **1980**, *38*, 75.
(30) Schreiber, A.; Ketelsen, I.; Findenegg, G. H. *Phys. Chem. Chem. Phys.* **2001**, *3*, 1185.
(31) Bogdanovič, B.; Brand, R. A.; Marjanovič, A.; Schwickardi, M.; Tölle, J. *J. Alloys Compd.* **2000**, *302*, 36.
(32) Ozolins, V.; Majzoub, E. H.; Udovic, T. J. *J. Alloys Compd.* **2004**, *375*, 1.

JP910511G